SCIENTIFIC REPORTS

OPEN

G-protein Gα_{13} functions as a cytoskeletal and mitochondrial regulator to restrain osteoclast function

Shinichi Nakano[1], Kazuki Inoue[1,2], Cheng Xu[1], Zhonghao Deng[1,3], Viktoriya Syrovatkina[4], Gregory Vitone[1], Liang Zhao[3], Xin-Yun Huang[4] & Baohong Zhao [1,2,5]

Excessive osteoclastic bone erosion disrupts normal bone remodeling and leads to bone loss in many skeletal diseases, including inflammatory arthritis, such as rheumatoid arthritis (RA) and psoriatic arthritis, periodontitis and peri-prosthetic loosening. Functional control of osteoclasts is critical for the maintenance of bone homeostasis. However, the mechanisms that restrain osteoclast resorptive function are not fully understood. In this study, we identify a previously unrecognized role for G-protein Gα_{13} in inhibition of osteoclast adhesion, fusion and bone resorptive function. Gα_{13} is highly expressed in mature multinucleated osteoclasts, but not during early differentiation. Deficiency of Gα_{13} in myeloid osteoclast lineage (*G$\alpha_{13}^{\Delta M/\Delta M}$ mice*) leads to super spread morphology of multinucleated giant osteoclasts with elevated bone resorptive capacity, corroborated with an osteoporotic bone phenotype in the *G$\alpha_{13}^{\Delta M/\Delta M}$ mice*. Mechanistically, Gα_{13} functions as a brake that restrains the c-Src, Pyk2, RhoA-Rock2 mediated signaling pathways and related gene expressions to control the ability of osteoclasts in fusion, adhesion, actin cytoskeletal remodeling and resorption. Genome wide analysis reveals cytoskeleton related genes that are suppressed by Gα_{13}, identifying Gα_{13} as a critical cytoskeletal regulator in osteoclasts. We also identify a genome wide regulation of genes responsible for mitochondrial biogenesis and function by Gα_{13} in osteoclasts. Furthermore, the significant correlation between Gα_{13} expression levels, TNF activity and RA disease activity in RA patients suggests that the Gα_{13} mediated mechanisms represent attractive therapeutic targets for diseases associated with excessive bone resorption.

Bone destruction is a major cause of disability associated with many skeletal diseases, such as rheumatoid arthritis (RA), psoriatic arthritis, periodontitis and peri-prosthetic loosening[1–5]. Osteoclasts are the exclusive cell type that is responsible for bone resorption. Excessive generation of osteoclasts or increased osteoclast activity leads to pathologic bone erosion. Osteoclasts differentiate from the monocyte/macrophage lineage. Osteoclastogenesis is induced by the master osteoclastogenic cytokine receptor activator of nuclear factor-κB ligand (RANKL), which acts in concert with macrophage colony-stimulating factor (M-CSF) and immunoreceptor tyrosine-based activation motif (ITAM)-mediated co-stimulatory signals. Binding of RANKL to its receptor RANK activates a broad range of signaling cascades, including canonical and non-canonical NF-κB pathways; mitogen-activated kinase (MAPK) pathways leading to the activation of AP-1 and CREB transcription factors; and calcium signaling, to induce the expression of key transcription factors Blimp1 and NFATc1 to initiate early stage of osteoclast differentiation[2,6–9].

[1]Arthritis and Tissue Degeneration Program and The David Z, Rosensweig Genomics Research Center, Hospital for Special Surgery, New York, New York, USA. [2]Department of Medicine, Weill Cornell Medical College, New York, New York, USA. [3]Department of Orthopedic Surgery, Nanfang Hospital, Southern Medical University, Guangzhou, Guangdong, China. [4]Department of Physiology and Biophysics, Weill Cornell Medical College, New York, New York, USA. [5]Graduate Program in Cell & Developmental Biology, Weill Cornell Graduate School of Medical Sciences, New York, New York, USA. Shinichi Nakano and Kazuki Inoue contributed equally. Correspondence and requests for materials should be addressed to B.Z. (email: zhaob@hss.edu)

Along the differentiation process, myeloid precursors first undergo differentiation to mononuclear osteoclasts, which then fuse into mature giant multinucleated polykaryons at late stages driven by the expression of genes responsible for cell-cell fusion, such as DC-Stamp and ATP6v0d2[10,11]. The giant multinucleated osteoclasts express high levels of osteoclast marker genes, such as Tartrate Resistant Acidic Phosphatase (*Acp5*), Cathepsin K (*CtsK*) and αvβ3 integrin (*Itgb3*). The expression of these genes is essential for mature osteoclasts to exert their major function, bone-resorption, through acid decalcification and proteolytic degradation of the bone matrix[2,9]. As a premise, the process of bone resorption requires osteoclasts to be polarized and to adhere tightly to the bone surface to form a unique structure, called the sealing zone, via actin ring formation surrounding a ruffled border. The unique osteoclastic actin ring structure makes the sealing zone an isolated resorptive microenvironment that concentrates the secreted protons and degrading enzymes for efficient resorption to occur[12–14]. Upon stimulation, such as attachment to integrins and/or cytokine activation by M-CSF or RANKL, osteoclasts undergo rapid cytoskeletal reorganization, appear polarized and form actin rings (the actin rings display as actin rings/belts in *in vitro* cultures)[14,15]. c-Src initiated signaling cascades including downstream activation of Syk, Pyk2 and small Rho GTPases are well studied and known to play important roles in actin reorganization[14,15]. Cytoskeletal reorganization in osteoclasts, mainly reflected by dynamic actin ring formation, is a prerequisite for osteoclast polarization, movement and bone resorptive function. Recent evidence shows that functional control of osteoclasts is important for the maintenance of bone homeostasis[16–19]. Nonetheless, the mechanisms regulating osteoclast cytoskeleton organization and function, especially the negative feedback mechanisms, remain underexplored.

G-protein mediated signaling pathways contribute to diverse cellular activities, such as cell growth, differentiation and survival. Guanine nucleotide-binding protein subunit alpha 13 (Gα$_{13}$; encoded by *Gna13*) is a member of the G12 subfamily of the heterotrimeric G proteins. These G-proteins include Gα, Gβ, and Gγ subunits and couple specific receptors to transduce signals to downstream effectors[20,21]. The G12 subfamily has two members, Gα$_{12}$ and Gα$_{13}$. Gα$_{13}$ is more critical than Gα$_{12}$ during development, demonstrated by the genetic evidence that mice with global knockout of Gα$_{13}$, but not Gα$_{12}$, exhibit embryonic lethality[22,23]. Gα$_{13}$ plays key roles in biological and disease settings, such as embryogenesis, angiogenesis, cell cytoskeleton organization, cellular transformation, and metastatic tumor progression[21]. In addition, Gα$_{13}$ can interact with other proteins to regulate different signaling pathways, such as MAPK pathway and the Rho GTPases[20]. Wu *et al.* recently reported that Gα$_{13}$ negatively regulates osteoclast differentiation through inhibition of the Akt-GSK3β-NFATc1 signaling[24]. Here, we identified a previously unrecognized expression pattern for Gα$_{13}$ and unique molecular mechanisms by which Gα$_{13}$ regulates osteoclast function. In contrast to a low expression level of Gα$_{13}$ in osteoclast precursors and early stages of differentiation, we found that Gα$_{13}$ is highly expressed in multinucleated osteoclasts, indicating a potential role for Gα$_{13}$ in mature osteoclasts. Given the critical roles for G12 proteins in regulating cytoskeleton in fibroblasts and endothelial cells[25–28], it would be of interest and importance to explore whether Gα$_{13}$ regulates osteoclast cytoskeletal reorganization and function.

In the present study, we found that Gα$_{13}$ is a RANKL-inducible G-protein that is highly expressed in multinucleated osteoclasts and plays an important feedback inhibitory role in controlling osteoclast actin ring formation and resorptive function. We found that Gα$_{13}$ deficiency in myeloid lineage does not affect early stages of osteoclast differentiation, but enhances gene expression responsible for osteoclast fusion, resorption and cytoskeletal reorganization. The inducible Gα$_{13}$ expression pattern in multinucleated osteoclasts may explain its stage-dependent function. Compared to the wild type (WT) cells, the Gα$_{13}$ conditional knockout (KO) osteoclasts show super spread giant multinucleated morphology both *in vitro* and *in vivo* with rapid actin ring reorganization and increased bone resorption. Osteoclast cytoskeletal organization and resorption is a highly energy consuming process. The enhanced osteoclast function was further corroborated by highly enriched expression of genes involved in cytoskeleton, mitochondrial biogenesis and function in Gα$_{13}$ conditional KO osteoclasts by genome wide analysis of gene expression and Gene Oncology (GO) analysis. Collectively, our findings uncovered a novel function of Gα$_{13}$ that acts as a cytoskeletal and mitochondrial regulator to play a feedback inhibitory role in osteoclast fusion, cytoskeletal reorganization and function. Furthermore, we found that Gα$_{13}$ expression is inversely correlated with TNF and RA disease activity, suggesting that appropriate modulation of Gα$_{13}$ would provide an alternative strategy to control osteoclast function thereby preventing bone loss.

Results

Gα$_{13}$ is a RANKL inducible gene that controls osteoclast size and resorptive function.
Global deletion of Gα$_{13}$ expression in mice leads to embryonic lethality[22,23]. Thus, to determine the role of Gα$_{13}$ in osteoclastogenesis, we deleted *Gna13* (encoding Gα$_{13}$) in myeloid lineage osteoclast precursors by crossing *Gα$_{13}$^{flox/flox}* mice with *LysMcre* mice that express Cre under the control of the myeloid-specific lysozyme M promoter. We used *Gα$_{13}$^{flox/flox}LysMcre*(+) mice (hereafter referred to as Gα$_{13}$^{ΔM/ΔM}) and littermate controls with a Gα$_{13}$^{+/+} *LysMcre*(+) genotype (hereafter referred to as wild type (WT)) in the experiments. The bone marrow derived macrophages (BMMs) were used as osteoclast precursors *in vitro*. We first examined the mRNA and protein expression levels of Gα$_{13}$ during osteoclast differentiation induced by RANKL, a master osteoclastogenic cytokine. We observed that low Gα$_{13}$ expression levels were maintained throughout the early stage of differentiation and were not highly induced until three days after RANKL stimulation, when the cells generally started fusion and became mature multinucleated giant osteoclasts in cultures (Fig. 1A,B). This inducible Gα$_{13}$ expression pattern indicates its potential dominant role presumably in the late stage of osteoclast differentiation. Indeed, we found that Gα$_{13}$^{ΔM/ΔM} derived BMMs formed nearly similar number of TRAP-positive multinucleated osteoclasts, but strikingly increased the average osteoclast area to approximately three times of that of the WT cells (Fig. 1C,D). The average numbers of nuclei per TRAP-positive MNC in Gα$_{13}$^{ΔM/ΔM} osteoclasts were significantly greater than those in WT osteoclasts (Fig. 1D), indicating a suppressive role for Gα$_{13}$ in cell fusion. The Gα$_{13}$^{ΔM/ΔM} osteoclast area began to increase after three days of RANKL stimulation and increased more drastically after four or five days of RANKL stimulation (Fig. 1E). The super spread Gα$_{13}$^{ΔM/ΔM} multinucleated osteoclasts formed
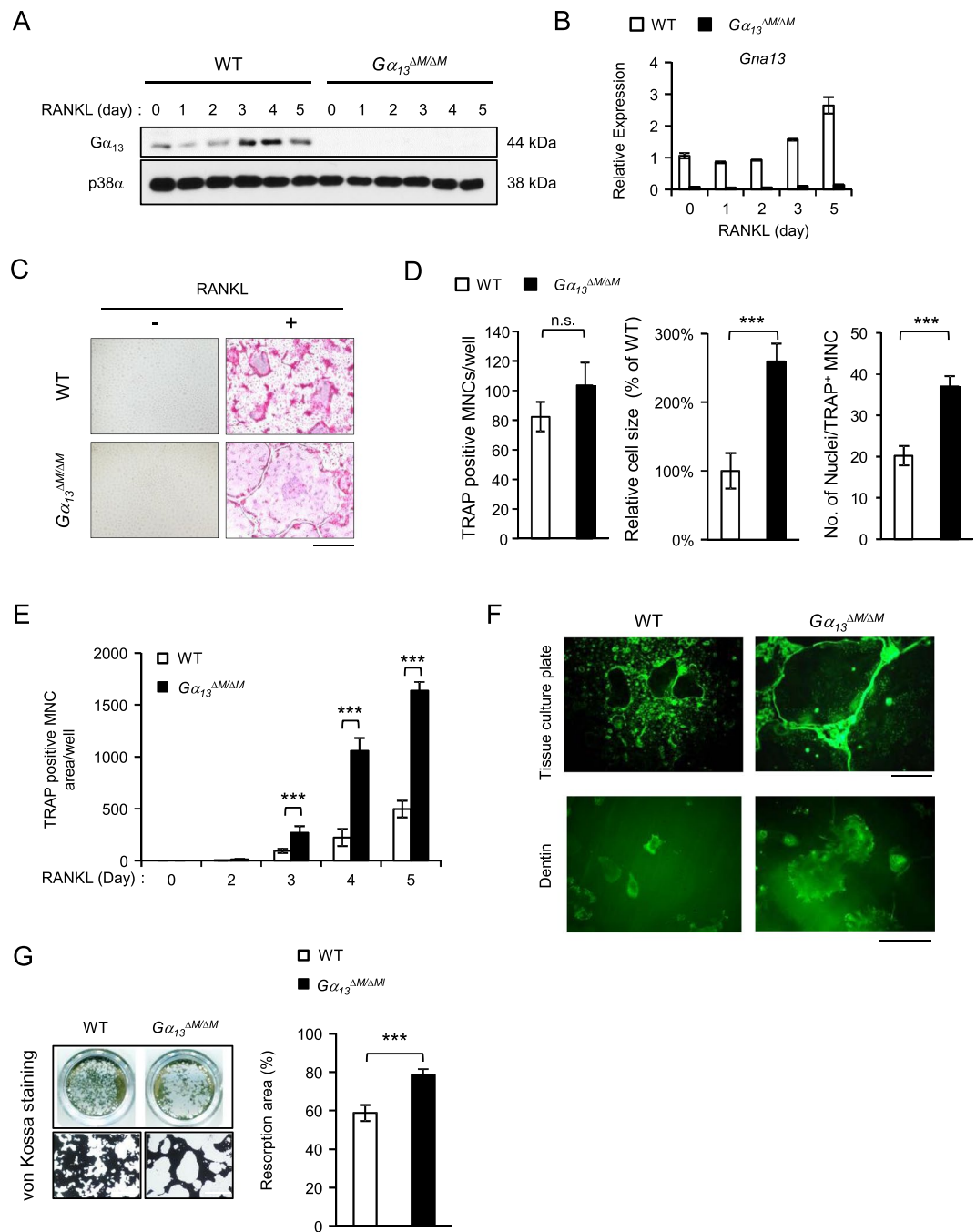
Figure 1. Gα₁₃ is a RANKL inducible inhibitor that restrains osteoclast size and resorptive activity.
(**A**) Immunoblot analysis and (**B**) quantitative real-time PCR analysis of mRNA *(Gna*13*)* expression of Gα$_{13}$
induced by RANKL. (**C**) Osteoclast differentiation using BMMs derived from WT and *Gα$_{13}^{ΔM/ΔM}$* mice
stimulated with RANKL for five days. TRAP staining was performed and TRAP-positive multinucleated cells
(MNCs) appear red in the photographs. Scale bar, 500 μm. (**D**) The number (left panel) and the relative average
size (middle panel) of TRAP-positive MNCs ($> = 3$ nuclei per cell) per well and the average numbers of nuclei
per TRAP-positive MNC (right panel) were quantified by Osteomeasure software. (**E**) Quantification of the
area of TRAP positive MNCs derived from WT and *Gα$_{13}^{ΔM/ΔM}$* at the indicated days in the presence of RANKL
(40 ng/ml). (**F**) Upper panel: Actin ring formation in the cell culture plates of BMMs derived from WT and
Gα$_{13}^{ΔM/ΔM}$ mice stimulated with RANKL for five days. Podosome belts are peripherally located. Scale bar,
500 μm. Lower panel: Actin ring formation on dentin slices of BMMs derived from WT and *Gα$_{13}^{ΔM/ΔM}$* mice
stimulated with RANKL for six days. Actin rings are peripherally or internally located. Scale bar, 100 μm.
(**G**) Mineral resorption activity of MNCs derived from WT and *Gα$_{13}^{ΔM/ΔM}$* mice. The BMMs were cultured on
the calcium coated plates with RANKL for seven days. Von kossa staining was performed to detect resorptive pit
areas. The representative images of whole well (upper) and 10× magnified field (lower) were shown in the left
panel. Scale bars = 500 μm. Quantification of resorptive area relative to whole well area was shown in the right
panel. All data are shown as mean ± S.D. ***$p < 0.001$, n.s., not statistically significant.

F-actin rings (podosome belts) on both tissue culture plates and dentin slices (Fig. 1F) and were functional in mineral resorption (Fig. 1G). Consistent with the osteoclast area, the resorptive area generated by the $G\alpha_{13}{}^{\Delta M/\Delta M}$ cells was much larger than that by the WT osteoclasts (Fig. 1G). Notably, the super spread giant osteoclasts were also observed in the $G\alpha_{13}{}^{\Delta M/\Delta M}$ mice (Fig. 2A). Similarly as in the *in vitro* cultures, $G\alpha_{13}$ deficiency did not result in different osteoclast numbers *in vivo*. Significantly, the average osteoclast size and the relative osteoclast surface to bone surface were both enhanced in the $G\alpha_{13}{}^{\Delta M/\Delta M}$ mice (Fig. 2B). We furthermore examined the serum levels of TRAP and C-terminal telopeptide of type 1 collagen (CTX-I), which are important indicators reflecting osteoclast activity *in vivo*. As shown in Fig. 2C,D, both serum TRAP and CTX-I levels were significantly elevated in the $G\alpha_{13}{}^{\Delta M/\Delta M}$ mice. We next performed microcomputed tomographic (μCT) analyses in order to examine whether the super spread $G\alpha_{13}{}^{\Delta M/\Delta M}$ osteoclasts have effects on the bone phenotype. As shown in Fig. 3, $G\alpha_{13}{}^{\Delta M/\Delta M}$ mice exhibit the osteoporotic phenotype indicated by decreased trabecular bone volume, number, bone mineral density and increased trabecular bone spacing. Taken together with the enhanced osteoclast surface and size *in vivo* in $G\alpha_{13}{}^{\Delta M/\Delta M}$ mice, these data demonstrate that the resorptive function of the super spread $G\alpha_{13}{}^{\Delta M/\Delta M}$ osteoclasts is significantly enhanced, leading to an osteoporotic bone phenotype. Collectively, our results identify a previously unrecognized role for $G\alpha_{13}$ that controls the size of osteoclasts during the late stage of osteoclast differentiation. Deficiency of $G\alpha_{13}$ leads to super spread morphology of multinucleated giant osteoclasts with elevated bone resorptive capacity.

$G\alpha_{13}$ deficiency affects the expression of genes responsible for osteoclast terminal differentiation and function. We next investigated the molecular mechanisms by which $G\alpha_{13}$ regulates osteoclast size and function. We first examined the expression of the genes that play key roles in osteoclast differentiation, fusion and resorptive function. Consistent with the phenotype that $G\alpha_{13}$ does not significantly change osteoclast numbers, $G\alpha_{13}$ deficiency did not alter the induction and expression levels of key osteoclastogenic genes induced by RANKL (Fig. 4A,B), such as *Fos* (encoding c-Fos), *Nfatc1* (encoding NFATc1) and *Prdm1* (encoding Blimp1), each of which is essential for early osteoclast differentiation. Furthermore, the early osteoclastogenic signaling pathways, such as NF-κB, MAPK and c-Fos, were activated similarly by RANKL between the WT and $G\alpha_{13}{}^{\Delta M/\Delta M}$ osteoclast precursors (data not shown). In addition, phosphorylation of AKT in response to M-CSF or RANKL was not affected by $G\alpha_{13}$ (Supplementary Fig. 1). These results collectively support the phenotype that $G\alpha_{13}$ does not affect early stage of osteoclast differentiation. On the other hand, the genes that control osteoclast function, such as *CTR* (encoding calcitonin receptor), *Ctsk* (encoding cathepsin K), *Acp5* (encoding TRAP) and *Itgb3* (encoding integrin β3), were significantly enhanced by RANKL in $G\alpha13$ deficient cell cultures (Fig. 4A). These findings provide a molecular basis for the enhanced bone resorptive function of $G\alpha_{13}$ deficient osteoclasts. Cell fusion process regulates osteoclast size. Following this line, we found that the expression levels of the genes responsible for osteoclast fusion, *Dc-stamp* (encoding DC-STAMP) and *Atp6v0d2* (encoding ATP6v0d2), were higher in $G\alpha_{13}{}^{\Delta M/\Delta M}$ osteoclasts than WT cells (Fig. 4A). The negative regulation of these cell-cell fusion genes by $G\alpha_{13}$ might be responsible, at least partially, for the super spread morphology of $G\alpha_{13}{}^{\Delta M/\Delta M}$ osteoclasts with large sizes.

$G\alpha_{13}$ regulates cytoskeletal reorganization in osteoclasts. In addition to gene expression, cytoskeletal reorganization, including cellular adhesion to bone surface and actin ring (podosome belt) formation to generate an isolated resorptive microenvironment (sealing zone), is essential for osteoclasts to effectively execute their bone resorbing function. Moreover, dynamic remodeling of actin cytoskeleton is critical for osteoclasts to cycle actively between resorption-migration-resorption phases on the bone surface. The integrin- or cytokine-mediated cytoskeletal organization is mainly activated via a canonical signaling pathway, which is initiated by c-Src activation. Therefore, we first examined the levels of phosphor-c-Src, an indicator of c-Src activity. To determine the role of $G\alpha_{13}$ in the activation of c-Src in response to the integrin-mediated adhesion and signaling, we lifted and then re-plated WT or $G\alpha_{13}{}^{\Delta M/\Delta M}$ osteoclasts on culture dishes coated with fibronectin, which binds to cellular integrins and activates integrin-medicated signaling. We found that the phosphorylation of c-Src appeared much stronger in the $G\alpha_{13}{}^{\Delta M/\Delta M}$ cell cultures in response to adhesion than in the WT cultures, and was maintained at higher levels in the $G\alpha_{13}{}^{\Delta M/\Delta M}$ cell cultures (Fig. 5A). In addition, Pyk2 phosphorylation is critical for osteoclast adhesion, spreading and bone resorption. Phosphor-Erk and phosphor-FAK levels also play important roles in focal adhesion signaling and the regulation of osteoclast cytoskeletal reorganization[14,15,29]. Similarly as the regulation of c-Src activity, $G\alpha_{13}$ deficiency significantly elevated the adhesion-induced phosphorylation levels of Pyk2, FAK and Erk (Fig. 5A). Next, we investigated whether $G\alpha_{13}$ regulates the activity of Rho GTPases, the downstream effectors of these signaling pathways and central players in cytoskeleton reorganization. We found that $G\alpha_{13}$ deficiency increased the GTP bound RhoA levels in response to osteoclastic adhesion (Fig. 5B), consistent with the upstream signaling enhancement. The GTP-Rac1 level was not much affected by the absence of $G\alpha_{13}$ (data not shown). These results indicate that $G\alpha_{13}$ is an inhibitor of RhoA activity during cytoskeletal remodeling in osteoclasts. Rho-associated kinase Rock2 is a key downstream effector of RhoA. In parallel to the changes of RhoA activity, the phosphorylation levels at S1366 of Rock2, an indicator of its activation, were enhanced by $G\alpha_{13}$ deletion (Fig. 5A). These results further support an inhibitory role for $G\alpha_{13}$ in controlling the RhoA-Rock2 pathway during cytoskeleton organization in osteoclasts.

Furthermore, we investigated whether $G\alpha_{13}$ regulates dynamic remodeling of actin cytoskeleton. To address this question, we tested the cytokine-mediated actin ring re-organization of osteoclasts. The WT and $G\alpha_{13}{}^{\Delta M/\Delta M}$ osteoclast cultures were starved of M-CSF and RANKL. Five hours later, as expected with the knowledge of the importance of cytokine in cytoskeleton organization, the actin rings disappeared in both WT and $G\alpha_{13}{}^{\Delta M/\Delta M}$ osteoclast cultures on tissue culture plates or on dentin slices (Fig. 5C,D, time 0 after starvation). Upon re-stimulation with M-CSF and RANKL, $G\alpha_{13}$ deficiency enabled the cells to reorganize the actin cytoskeleton to form actin rings within 5 minutes, which was much faster than the WT cells that needed 30 minutes (Fig. 5C).
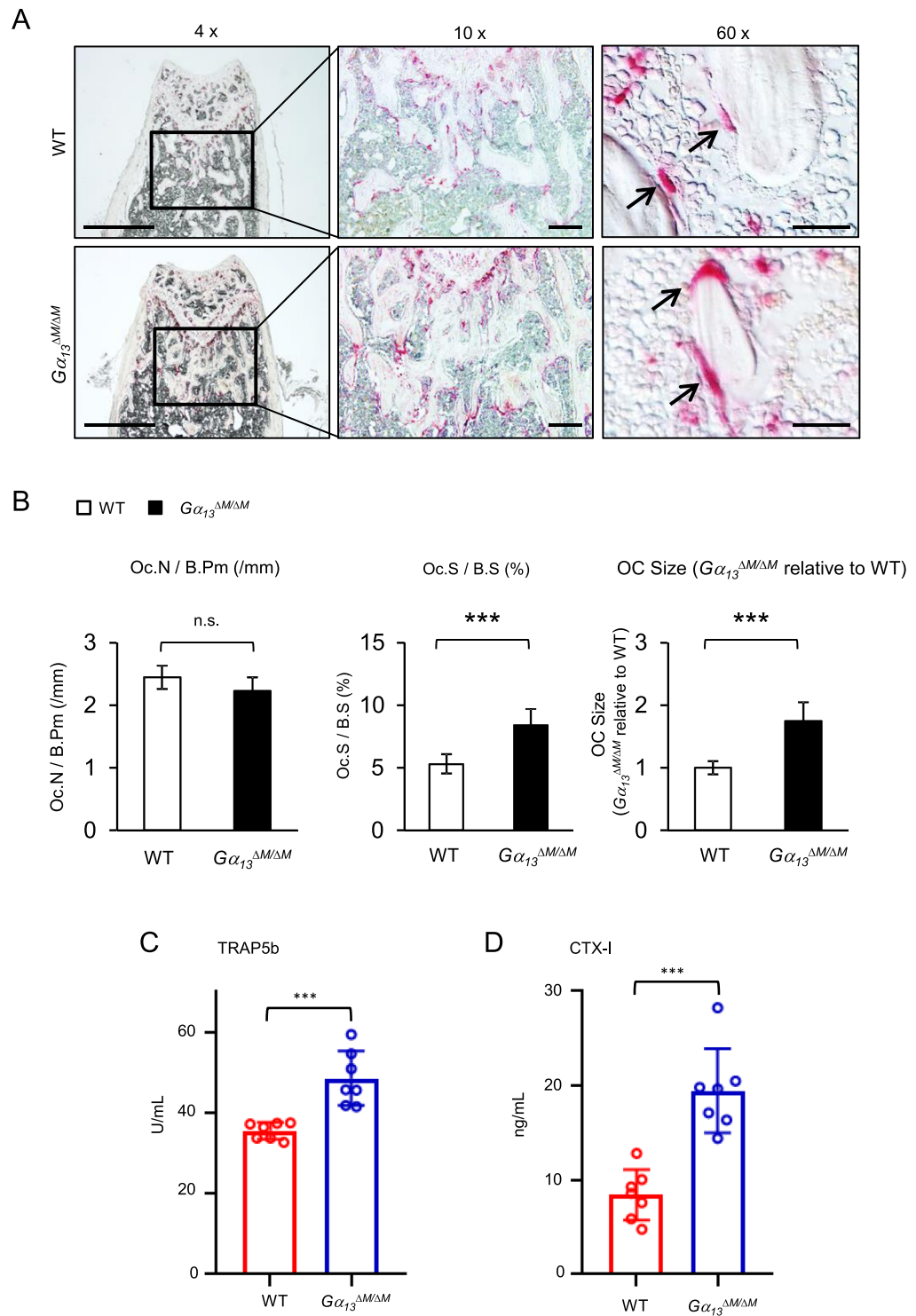
Figure 2. Gα₁₃ deficiency increases osteoclast size but not numbers *in vivo*. TRAP staining (**A**) and histomorphometric analysis (**B**) of histological sections obtained from the metaphysis region of distal femurs of two-month-old male $G\alpha_{13}^{\Delta M/\Delta M}$ mice and their littermate WT control mice. Scale bars = 1 mm (4 × objective), 200 μm (10 × objective) or 20 μm (60 × objective) respectively. Oc.S/BS, osteoclast surface per bone surface; Oc. N/B.Pm, number of osteoclasts per bone perimeter. OC size, osteoclast surface divided by osteoclast number. Serum TRAP (**C**) and CTX-I (**D**) levels measured in the serums obtained from 8–12 week old age and gender both matched $G\alpha_{13}^{\Delta M/\Delta M}$ mice and their littermate WT control mice. n = 7. All data are shown as mean ± S.D. ***p < 0.001, n.s., not statistically significant.
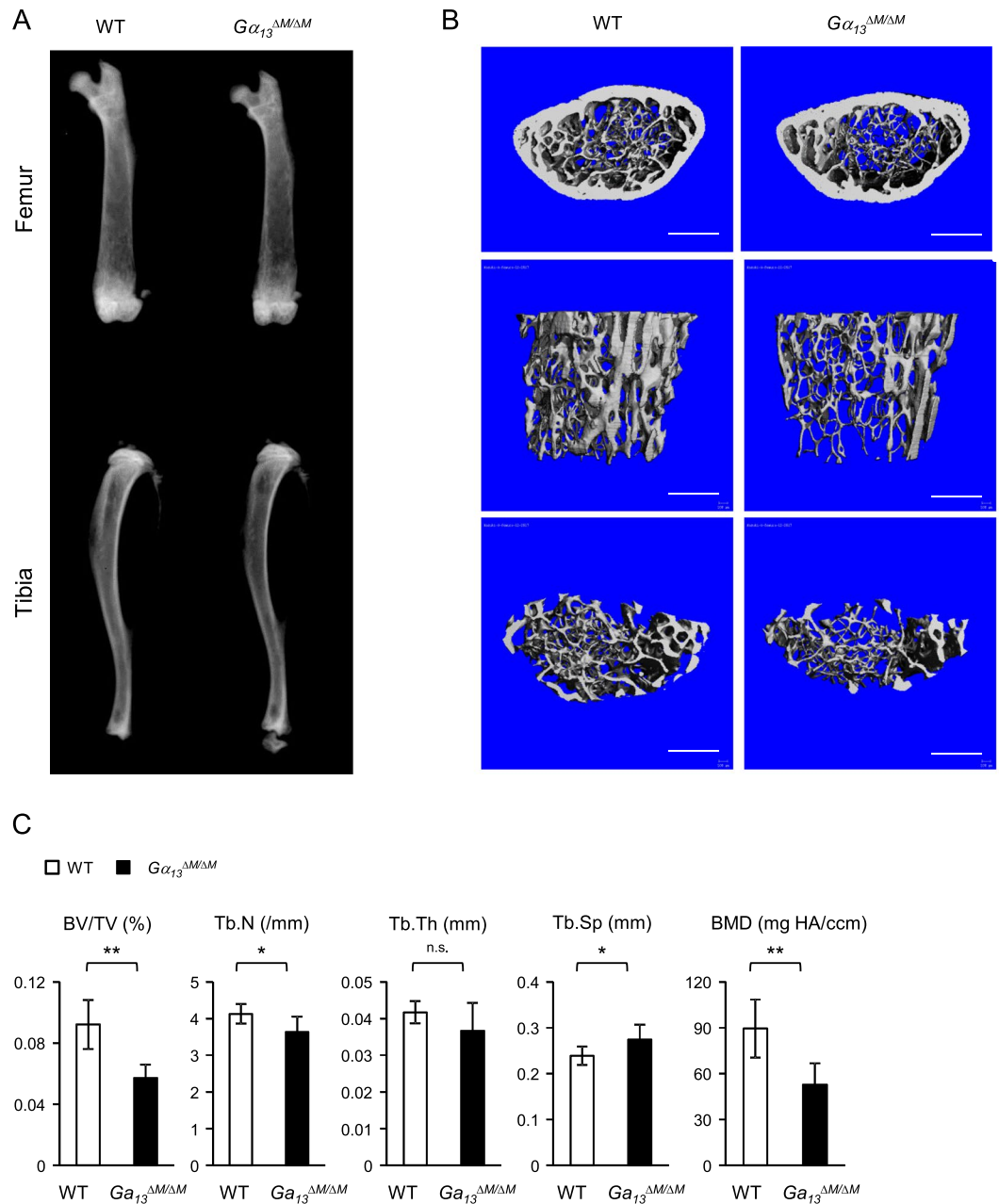
Figure 3. $G\alpha_{13}{}^{\Delta M/\Delta M}$ mice exhibit osteoporotic phenotype. (**A**) Radiographs of femurs and tibia, (**B**) μCT images and (**C**) bone morphometric analysis of the trabecular bone of the distal femurs isolated from two-month-old WT and $G\alpha_{13}{}^{\Delta M/\Delta M}$ male mice. Scale bar = 500 μm. n = 6 per group. All data are shown as mean ± S.D. $*p < 0.05$, $**p < 0.01$, n.s., not statistically significant. BV/TV, bone volume per tissue volume; Tb.N, trabecular number; Tb.Th, trabecular bone thickness; Tb.Sp, trabecular bone spacing, BMD, bone mineral density.

On dentin slices, reorganized actin rings formed significantly more in $G\alpha_{13}{}^{\Delta M/\Delta M}$ osteoclast cultures than in WT cultures after 30 minutes of restimulation with M-CSF and RANKL (Fig. 5D). These findings collectively indicate that $G\alpha_{13}$ functions as a brake that restrains the signaling pathways mediated by Src, Pyk2, Erk, FAK and RhoA-Rock2, which are important for cytoskeleton remodeling, such as in the process of adhesion, actin reorganization and actin-ring formation. $G\alpha_{13}$, a RANKL inducible inhibitor, thus plays a feedback inhibitory role in cytoskeletal reorganization in osteoclasts.

Genome wide analysis reveals that Gα₁₃ regulates key genes responsible for cytoskeleton, mitochondrial biogenesis and function. To further explore molecular mechanisms by which $G\alpha_{13}$ acts on osteoclast function, we performed gene expression profiling using high throughput sequencing of RNA (RNAseq) with the WT and $G\alpha_{13}{}^{\Delta M/\Delta M}$ osteoclast precursors at baseline and the corresponding osteoclasts after RANKL stimulation for five days to identify genes regulated by $G\alpha_{13}$. We next performed Gene Ontology (GO)
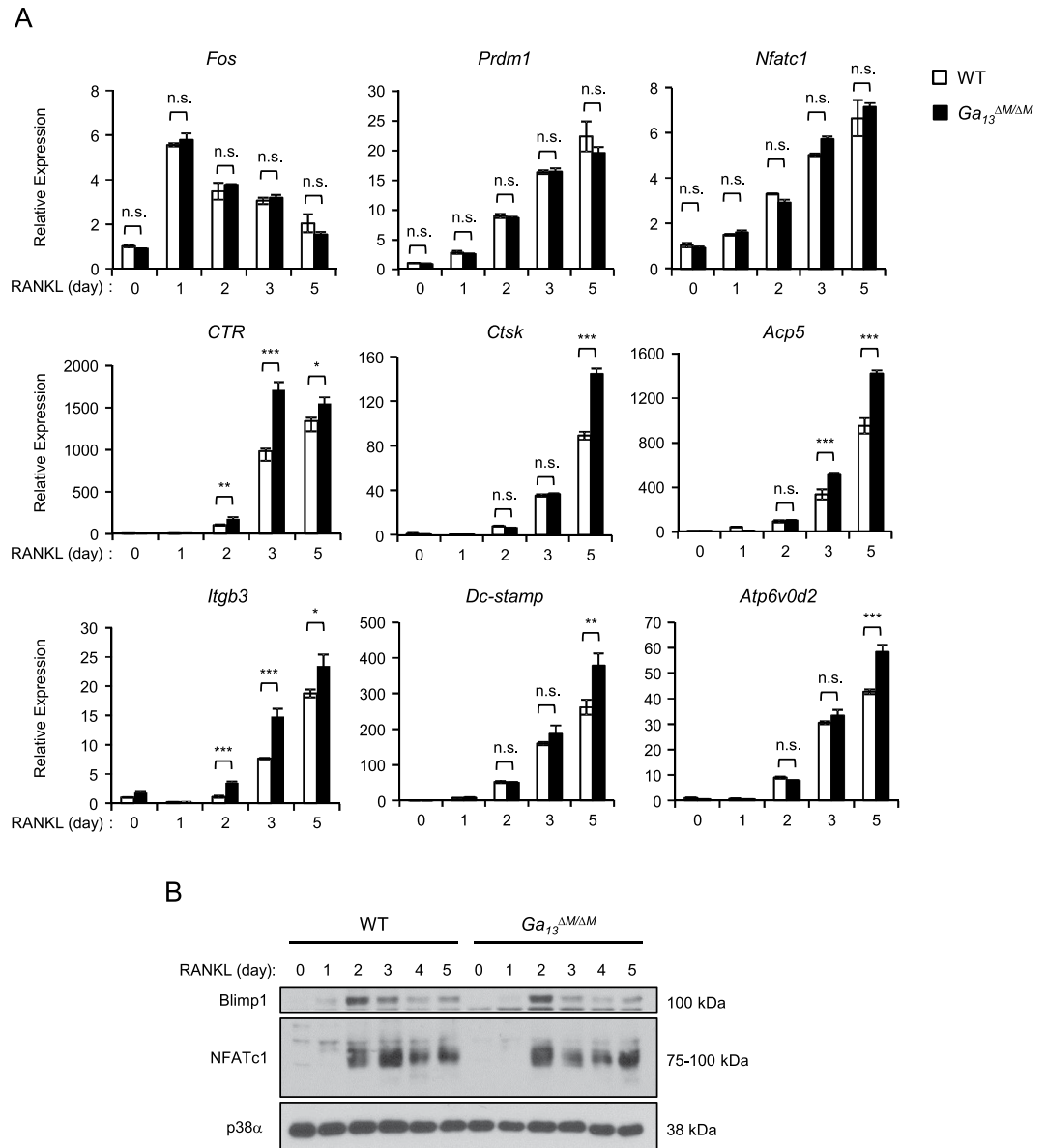
A

B

Figure 4. Gα$_{13}$ selectively suppresses the expression of genes responsible for osteoclast function and fusion, but not for early differentiation. (**A**) Quantitative real-time PCR analysis of mRNA expression of *Fos (encoding c-Fos)*, *Prdm1* (encoding Blimp1), *Nfatc1* (encoding NFATc1), *CTR* (encoding calcitonin receptor), *Ctsk* (encoding cathepsin K), *Acp5* (encoding TRAP), *Itgb3* (encoding integrin β3), *Dc-stamp* (encoding DC-stamp) and *Atp6v0d2* (encoding ATP6v0d2) in WT and *Gα$_{13}$*$^{ΔM/ΔM}$ osteoclast cultures induced by RANKL at the indicated times. (**B**) Immunoblot analysis of the expression of Blimp1 and NFATc1 in WT and *Gα$_{13}$*$^{ΔM/ΔM}$ osteoclast cultures induced by RANKL at the indicated times. p38α was used as a loading control. All data are shown as mean ± S.D. *$p < 0.05$, **$p < 0.01$, ***$p < 0.001$, n.s., not statistically significant.

analysis of the up-regulated genes in the RANKL stimulation condition in the *Gα$_{13}$*$^{ΔM/ΔM}$ osteoclasts. Consistent with the phenotype of the enhanced ability of *Gα$_{13}$*$^{ΔM/ΔM}$ osteoclasts for adhesion and actin ring organization, GO analysis revealed highly significant upregulation of genes involved in cytoskeleton, ruffle and adhesion (Fig. 6A). We further extracted the gene expression values and found that 307 cytoskeleton-related genes (Fig. 6B, Supplementary Table 1), including *GIT1 and Itgb3*, were significantly elevated by Gα$_{13}$ deficiency. These genome wide analysis data provided another important piece of evidence for the regulatory role of Gα$_{13}$ in cytoskeleton reorganization. The profound effect of Gα$_{13}$ on the cytoskeleton gene expression indicates that Gα$_{13}$ likely functions as a central cytoskeleton regulator. As expected, the genes in charge of osteoclast differentiation, such as *Nfatc1*, *Fos*, *Prdm1*, were not affected by Gα$_{13}$ deficiency (data not shown).

Surprisingly, we found that the most enriched gene sets were involved in mitochondrial structural complex and mitochondrial respiratory chain complexes in Gα$_{13}$ deficient osteoclasts (Fig. 6A), indicating a negative regulation of mitochondrial biogenesis and function by Gα$_{13}$. We extracted these genes from the RNA-seq data and confirmed 51 mitochondrial related genes (Figs 6B, 7A) that were highly enhanced in the *Gα$_{13}$*$^{ΔM/ΔM}$ osteoclasts.

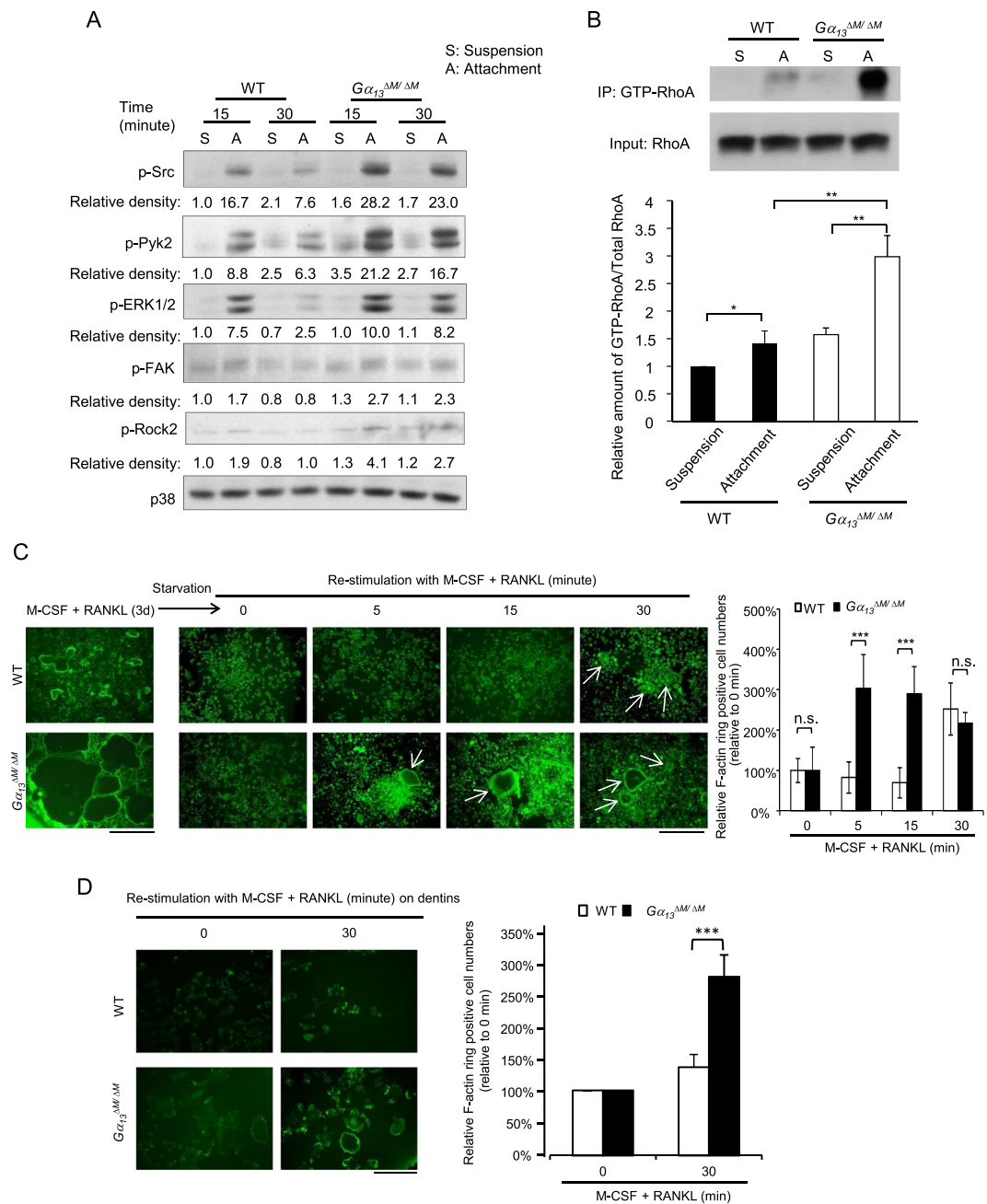**Figure 5.** Gα13 plays an inhibitory role in actin cytoskeleton organization in osteoclasts. Osteoclast differentiation of WT and $G\alpha_{13}^{\Delta M/\Delta M}$ BMMs was induced by RANKL for three days, the cells were starved in the culture medium without FBS, M-CSF and RANKL for 5 hours, and then the cells were lifted and replated onto Fibronectin-coated dishes for 15 or 30 min (A: attachment) or left in suspension (S: suspension), followed by the immunoblot analysis (**A**) of the expression of phospho-Src (Tyr416), phospho-Pyk2 (Thy402), phospho-ERK1/2 (Thr202/Tyr204), phospho-FAK (pY397) and phospho-Rock2 (Ser1366). p38α was used as a loading control. The relative density of each band to its corresponding loading control p38 band was calculated by Image J software, and then was normalized to the WT suspension condition (the 1st lane). (**B**) GTP-RhoA pulldown assay was performed using the 30 minute samples (a representative pulldown image, upper panel). The amount of GTP-bound RhoA was normalized to the total amount of RhoA (relative immunoblot band density) in cell lysates for the comparison of RhoA activity in different samples (lower panel). n = 3. Data are shown as mean ± S.D. *$p < 0.05$, **$p < 0.01$. (**C,D**) F-actin phalloidin staining (left panel) of non-starved cell cultures stimulated with M-CSF and RANKL for three days (C, on the tissue culture plates), or the cell cultures starved for five hours followed by re-stimulation with M-CSF and RANKL for the indicated times (C, on the tissue culture plates; D, on dentin slices). Scale bar in C, 500μm. Scale bar in D, 100 μm. Quantification of the relative numbers of F-actin ring positive cells to their corresponding time 0 condition was shown in the right panels. All data are shown as mean ± S.D. ***$p < 0.001$, n.s., not statistically significant.
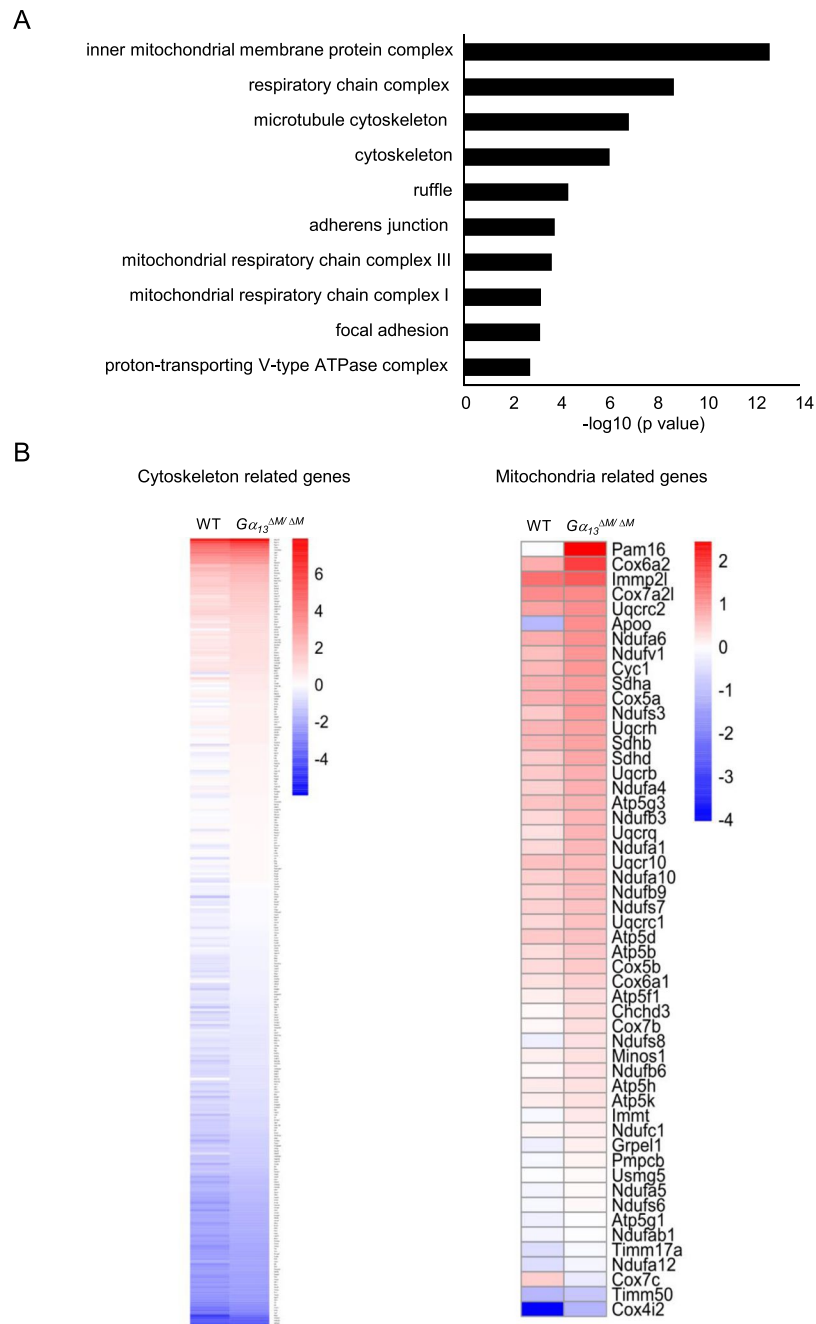
Figure 6. Genome wide analysis shows that $G\alpha_{13}$ selectively restrains the cytoskeleton and mitochondrial gene expression in osteoclasts. RNA sequencing was performed using the mRNAs extracted from the WT and $G\alpha_{13}^{\Delta M/\Delta M}$ BMMs stimulated with or without RANKL for five days. (**A**) Gene ontology analysis of RANKL-induced and $G\alpha_{13}$ deficiency-enhanced genes performed by PANTHER classification system. (**B**) RNAseq–based expression heat map of the RANKL-induced cytoskeleton related genes (Left panel) and mitochondria related genes (Right panel) regulated by $G\alpha_{13}$ deficiency. The log2 values of the fold changes of TPMs (RANKL condition relative to the non-stimulation control) are shown in the heat map.

These findings obtained from genome wide analysis highlight an exciting and promising novel regulatory network in osteoclasts mediated by $G\alpha_{13}$ on mitochondrial regulation. Since osteoclast resorption is a highly energy consuming process, the enhanced osteoclast activities in the absence of $G\alpha_{13}$, including cytoskeleton organization, remodeling and resorption, would require and be supported by increased energy supply from mitochondria. While we were preparing our manuscript, the Zou and Teitelbaum group showed that mitochondria mediated cytoskeleton organization contributes to osteoclast resorptive function[30]. In osteoclasts, we also found that $G\alpha_{13}$ deficiency enhanced mitochondrial DNA content (Fig. 7B), reflecting an increase in mitochondrial biogenesis. These results, together with the enhanced expression of genes for controlling mitochondrial biogenesis and
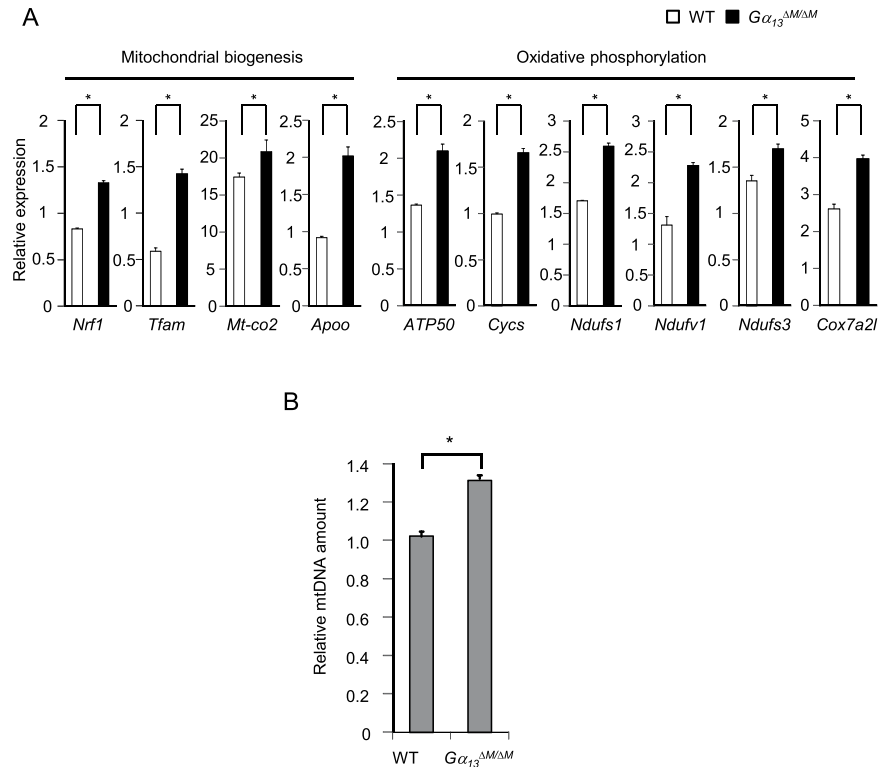
Figure 7. Gα₁₃ regulates mitochondrial biogenesis and function and contributes to mitochondrial-mediated actin organization in osteoclasts. (**A**) Quantitative real-time PCR analysis of gene expression responsible for mitochondrial biogenesis and oxidative phosphorylation. (**B**) Relative mitochondrial DNA (mtDNA) amount to chromatin DNA amount. The amount of mitochondrial/chromosol DNA was measured by qPCR analysis for the Cytb gene and Hes1 gene loci using total DNA isolated from the osteoclasts stimulated by RANKL for four days. All data are shown as mean ± S.D. **$p < 0.001$, n.s., not statistically significant.

oxidative phosphorylation in the $G\alpha_{13}^{\Delta M/\Delta M}$ osteoclasts (Figs 6B, 7A), indicate that Gα₁₃ might suppress mitochondrial biogenesis and function, which provide energy supply in osteoclasts. Our findings are corroborated by a recent study demonstrating that Gα₁₃ negatively regulates mitochondrial gene expression and function in muscle cells[31]. These results together suggest a novel function for Gα₁₃ in the regulation of mitochondria in different cell types. Since mitochondria-provided energy is essential for every cellular function, there is a technical limitation to suppress mitochondrial function while without affecting cellular activity. Thus, we cannot exclude the possibility that the enhanced mitochondrial gene expression is an associated phenomenon along with the enhanced osteoclast function in the Gα₁₃ deficient osteoclasts. Nonetheless, although it is unclear whether the regulation is direct or indirectly associated, our results at least indicate that the genes related with mitochondrial biogenesis and function are regulated by Gα₁₃.

Gα₁₃ expression is down-regulated in RA and inversely correlated with RA activity. Having established that Gα₁₃ negatively regulates osteoclast resorptive function, we wished to examine whether Gα₁₃ expression levels are altered in the RA disease, in which excessive osteoclastic bone resorption is a hallmark of the characteristic pathogenesis of the disease. Similarly as in the mouse system, Gα₁₃ expression was highly induced in the human osteoclast precursors derived from CD14(+) peripheral blood monocytes (PBMCs) after a few days of RANKL stimulation (Supplementary Fig. 2). Strikingly, Gα₁₃ expression level was decreased in the CD14(+) PBMCs isolated from RA patients compared to healthy donors (Fig. 8A). Our findings suggest that the down-regulated Gα₁₃ expression in RA cells can result in the loss of a constraint on osteoclast function based on our data from mouse cells and that this effect could contribute to the pathogenic mechanism mediated by Gα₁₃ in the inflammatory bone resorption. Given the importance of TNF in the pathogenesis of RA and the resounding success of TNF blockade therapy (TNFi) in the treatment of RA, we first examined the Gα₁₃ effect on the TNF-mediated inflammatory osteoclast formation. In inflammatory conditions, TNF often acts in synergy with RANKL to promote osteoclastogenesis. To mimic the *in vivo* condition, we treated the BMMs with TNF in the presence of RANKL, and found that Gα₁₃ deletion also significantly promoted the areas of the TRAP (+) multinucleated osteoclasts (Supplementary Fig. 3), indicating that Gα₁₃ plays an inhibitory role in controlling osteoclast spreading in TNF-mediated inflammatory conditions. Furthermore, TNF blockade therapy of RA patients with a humanized antibody that specifically blocks TNF activity (Enbrel) strikingly elevated Gα₁₃ expression levels in the PBMCs after one or two month-treatment (Fig. 8B). Moreover, the therapeutic reduction of TNF activity by TNFi significantly increased Gα₁₃ expression levels in each individual RA patient after TNFi treatment (Fig. 8C). TNFi therapy decreases TNF activity in the pathogenesis of RA. Therefore, Gα₁₃ expression levels were
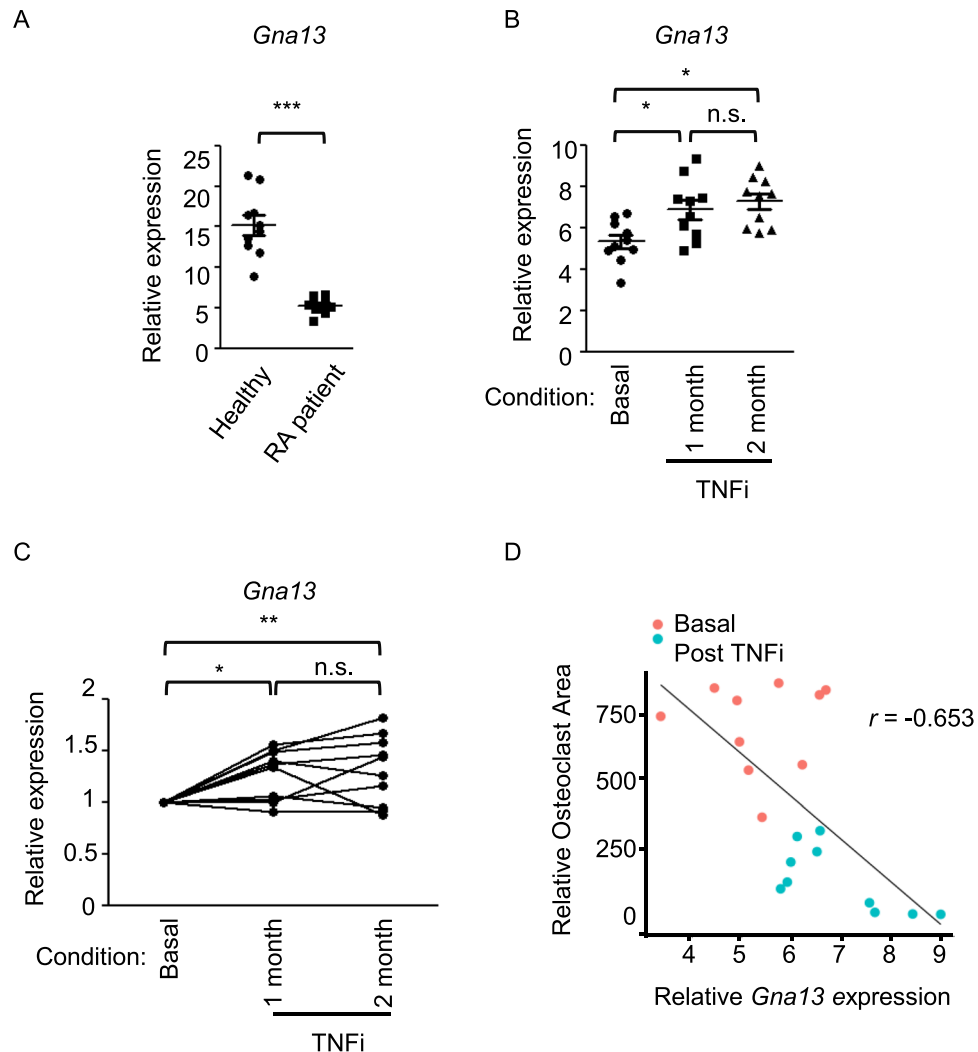
Figure 8. The expression levels of human Gα₁₃ are strongly correlated with RA disease. (**A**) Quantitative real-time PCR analysis of human Gα₁₃ (Gna13) expression in PBMCs isolated from healthy donors and RA patients. n = 10 for each group. Data are mean ± SEM. (**B**) Quantitative real-time PCR analysis of Gna13 expression in PBMCs isolated from RA patients before (basal level) and after TNFi therapy (Enbrel) for 1 and 2 months. (**C**) Quantitative real-time PCR analysis of the relative expression of Gna13 in PBMCs isolated from the same RA patient prior and after TNFi (Enbrel) for 1 and 2 months. Results were normalized to prior TNFi condition (basal) for each individual patient. (**D**) Scatter plot showing significant inverse correlation between the RA Gna13 expression levels and relative TRAP-positive osteoclast area in the cell cultures of RA CD14-positive PBMC-derived macrophages treated with RANKL (100 ng/ml) for five days. Each dot represents an RA patient in the indicated conditions. Plot was generated by ggplot2 statistical plotting package. Pearson's r = −0.653. *$p < 0.05$, **$p < 0.01$, ***$p < 0.001$, n.s., not statistically significant.

negatively correlated with TNF activity in RA. In parallel, TNFi significantly decreased the osteoclast areas of PBMCs (Fig. 8D). Further statistical analysis revealed a strong inverse correlation (Pearson's r = −0.653) between the levels of Gα₁₃ expression and the sizes of osteoclasts formed in RA PBMC cell cultures (Fig. 8D). Given the feedback effect of Gα₁₃ on osteoclast resorptive function, these findings support the idea that low Gα₁₃ levels in RA contribute to the pathologic osteoclastic bone erosion. Gα₁₃ expression levels are inversely correlated with the RA disease activity and thus could be a predictor of both osteoclast function and disease activity of RA.

Discussion

The adult skeleton undergoes constant and dynamic remodeling to maintain bone homeostasis, which is tightly regulated by osteoclast-mediated bone resorption and osteoblast/osteocyte-mediated bone formation[17,32,33]. This tightly-regulated balance is disrupted in the chronic inflammation and disease settings such as found in RA and periodontitis, which are some of the most common pathological conditions associated with bone loss. The balance disruption leads to excessive bone resorption and suppressed bone formation[1,3,4]. Clinical inhibition of osteoclast differentiation suppresses osteoclastic resorption, but meanwhile it often reduces osteoclast abundance. This pathological change dampens normal bone remodeling, resulting in insufficient bone formation in

multiple disease settings. Recent evidence shows the importance of appropriate maintenance of osteoclast abundance in balancing bone remodeling and stimulating new bone formation[16–19]. Thus, it comes under the spotlight to investigate how to control osteoclast function, which has not been fully understood. In this study, we identify a previously unrecognized role for $G\alpha_{13}$ in inhibition of osteoclast function. $G\alpha_{13}$ is selectively highly expressed in multinucleated osteoclasts during osteoclastogenesis. $G\alpha_{13}$ functions as a brake that restrains the signaling pathways and gene expression to control the ability of osteoclasts in fusion, adhesion, cytoskeletal remodeling and resorption. Deficiency of $G\alpha_{13}$ leads to an osteoporotic bone phenotype attributed to super spread osteoclasts with enhanced bone resorptive function. $G\alpha_{13}$ deletion does not affect osteoblast numbers and surfaces in mice (Supplementary Fig. 4). The close correlation between $G\alpha_{13}$ expression levels, TNF activity and RA disease activity in RA patients suggest that the $G\alpha_{13}$-pathway represents an attractive therapeutic target to prevent bone destruction in inflammatory diseases associated with excessive bone erosion.

Osteoclast cytoskeleton organization and remodeling, mainly reflected by actin ring and ruffled border formation, is crucial for the osteoclast bone resorptive ability. The defects in the canonical signaling pathways that positively regulate cytoskeleton organization, such as c-Src or Pyk2 deletion, often lead to abnormal actin ring assembly in osteoclasts with contracted morphology and low ability to resorb bone[12–15]. In contrast to these well-studied positive regulatory signals, the feedback regulatory mechanisms involved in cytoskeleton organization and osteoclast function remain poorly understood. The present study identifies $G\alpha_{13}$ as a newly identified negative regulator of osteoclast cytoskeleton organization and function. $G\alpha_{13}$ is a RANKL inducible inhibitor that generally reaches high expression levels after RANKL stimulation for a few days, but has marginal expression at early stage of differentiation before three days. The unique expression pattern of $G\alpha_{13}$ could explain its minimal effects on osteoclast differentiation.

Deletion of $G\alpha_{13}$ leads to enlarged super spread osteoclasts both *in vitro* and *in vivo*. These $G\alpha_{13}$ deficient osteoclasts have comparable survivability to WT cells (data not shown), but their abilities of fusion, adhesion, cytoskeleton organization and resorption are significantly enhanced. The underlying mechanisms include the negative regulation of gene expression that is in charge of cell-cell fusion and osteoclast function, c-Src, Pyk2, Erk and FAK mediated signaling and downstream activation of RhoA and ROCK2, as well as a unique mitochondrial regulation by $G\alpha_{13}$. Thus, the profound regulation of cytoskeleton by $G\alpha_{13}$ places $G\alpha_{13}$ in a central knot in the regulatory network mediating osteoclast function. Osteoclasts execute high energy-consuming activities, such as cellular adhesion, migration and bone resorption, all of which require appropriate cytoskeleton organization. To support sufficient energy consumption for these cellular activities, osteoclasts are a mitochondria-rich cell type. Thus, mitochondrial regulation would presumably affect cytoskeleton organization. Indeed, evidence[30] show that inhibition of mitochondrial function for a short period in osteoclasts almost completely disrupts actin ring structure. In this study, we identified the genome wide regulation of genes involved in mitochondrial biogenesis and function by $G\alpha_{13}$ in osteoclasts. This $G\alpha_{13}$ mediated regulation of mitochondria is also observed in muscle cells[31]. $G\alpha_{13}$ mediated mitochondrial function might contribute to the mechanisms by which $G\alpha_{13}$ restrains osteoclast cytoskeleton organization and function. It is however a puzzle how exactly $G\alpha13$ modulates gene expression in mitochondria. Conversely, cytoskeletal organization can influence mitochondrial network structure and function in certain cells, for example, mitochondria move along microtubules or actin filaments and actin filaments help determine the locations of mitochondria in neurons[34]. Thus, it seems that there is a cross-regulation between mitochondria and cytoskeleton. Although the mechanisms of the bi-directional regulation remain less understood, it is possible that the unique cytoskeletal structure in osteoclasts could regulate mitochondrial distribution and function. These interesting questions have not been explored and future studies would address whether and how mitochondria and cytoskeleton cross talk with each other. Overall, the findings from our genome wide study and another group[31] indicate a novel function of $G\alpha_{13}$ that contributes to the regulatory network of mitochondria and open a new avenue to study the biological significance and underlying mechanisms by which $G\alpha_{13}$ regulates mitochondria and cytoskeleton.

As a G-protein, $G\alpha_{13}$ can act through small Rho GTPases, such as Rac or RhoA, depending on cell types[20,25]. In osteoclasts, we found that $G\alpha_{13}$ functions through RhoA to further act on downstream Rock2. The $G\alpha_{13}$ mediated regulation of the RhoA-Rock2 pathway was also observed in muscle cells[31]. However, it is unclear how $G\alpha_{13}$ links to different GTPases and regulates their activity differently in various cells, presumably due to the various interactive proteins and guanine-nucleotide exchange factors (GEFs) in different settings[20,25,35]. The upstream GPCRs that connect to $G\alpha_{13}$, have not been identified in osteoclasts. We searched the GPCRs that were reported to play a part in osteoclasts, such as GPR103, EBI2, GPR68 and GPR55, and found that GPR55 is associated with $G\alpha_{13}$[36,37]. However, functional analysis *in vitro* could not provide clear evidence that GPR55 and $G\alpha_{13}$ work in the same pathway in osteoclasts (data not shown). It will be of interest and significance for future studies to investigate and uncover upstream regulators and receptors associated with $G\alpha_{13}$ in osteoclasts. Our study identified unique downstream factors, pathways and novel mitochondrial mediated mechanisms by which $G\alpha_{13}$ controls osteoclast cytoskeleton organization and function. $G\alpha_{13}$, as a novel negative regulator, plays a key role in the maintenance of osteoclast function. Given the deregulated $G\alpha_{13}$ levels in RA and its correlation with RA disease activity, targeting $G\alpha_{13}$ and its mediated pathways would provide alternative therapeutic strategies to control osteoclast function and excessive bone resorption associated with many diseases.

Materials and Methods

Animal study and analysis of bone phenotype.   We generated mice with myeloid specific deletion of $G\alpha_{13}$ by crossing $G\alpha13$ $^{flox/flox}$ mice[23] with mice with a lysozyme M promoter-driven Cre transgene on the C57BL/6 background (known as *LysMcre*; The Jackson Laboratory). Gender- and age-matched $G\alpha_{13}$ $^{flox/flox}$ *LysMcre*(+) mice (referred to as $G\alpha_{13}$ $^{\Delta M/\Delta M}$) and their littermates with *LysMcre*(+) genotype as wild-type controls (referred to as WT) were used for experiments. X-ray analysis was conducted using a high-resolution soft X-ray system (Faxitron Model MX-20) at 26 kV. Micro-computed tomography (μCT) analysis was conducted to evaluate bone

volume and 3D bone architecture using a Scanco μCT-35 scanner (SCANCO Medical) as described[38,39]. 2-month-old mouse femora were fixed in 10% buffered formalin and scanned at 6 μm resolution. Proximal femoral trabecular bone parameters were analyzed using Scanco software according to the manufacturer's instructions and the American Society of Bone and Mineral Research (ASBMR) guidelines. Femur bones were subjected to sectioning, TRAP staining, toluidine blue staining and histological analysis. Mouse serum TRAP was measured with MouseTRAP™ (TRAcP 5b) ELISA (Immunodiagnostic Systems (IDS)) and serum CTX-I was measured using Mouse CTX/Collagen C-Terminal Telopeptide ELISA Kit (LifeSpan BioSciences) according to manufacturer's instructions. The osteomeasure software (OsteoMetrics, Atlanta, GA, USA) was used for bone histomorphometry using standard procedures according to the program's instruction. All of the experiments were conducted according to the National Institutes of Health Guide for the Care and Use of Laboratory Animals. All animal studies were approved by the Hospital for Special Surgery Institutional Animal Care and Use Committee (IACUC), and Weill Cornell Medical College IACUC.

Reagents. Murine M-CSF, murine TNF and soluble human RANKL were purchased from PeproTech (Rochy Hill, NJ, USA). Recombinant Fibronectin was purchased from Sigma-Aldrich. Alexa Fluor® 488 phalloidin (A12379) was purchased from Invitrogen (Carlsbad, CA, USA).

Cell culture. To obtain bone marrow macrophages (BMMs), mouse bone marrow cells were harvested from tibiae and femora of age and gender-matched mutant and control mice and cultured for 3 days in α-MEM medium (Thermo Fisher Scientific) with 10% FBS (Atlanta Biologicals), glutamine (2.4 mM, Thermo Fisher Scientific), Penicillin-Streptomycin (Thermo Fisher Scientific) and CMG14-12 supernatant (condition medium, CM), which contained the equivalent of 20 ng/ml of rM-CSF and was used as a source of M-CSF as described[38]. The attached BMMs were scraped, seeded at a density of $4.5 \times 10^4/cm^2$, and cultured in α-MEM medium with 10% FBS, 1% glutamine and CM for overnight. Except where stated, the cells were then treated with or without optimized concentrations of RANKL (40 ng/ml) or TNF (40 ng/ml) in the presence of CM for times indicated in the figure legends. Culture media were exchanged every three days. Human osteoclast cultures were performed as described previously[40]. Briefly, peripheral blood mononuclear cells (PBMCs) from whole blood of healthy volunteers or RA patients were isolated by density gradient centrifugation using Ficoll (Invitrogen Life Technologies, Carlsbad, CA). CD14+ cells were purified from fresh PBMCs using anti-CD14 magnetic beads (Miltenyi Biotec, Auburn, CA) as recommended by the manufacturer. Human monocytes were cultured in α-MEM medium with 10% FBS in the presence of M-CSF (20 ng/ml; PeproTech, Rocky Hill, NJ) for 2 days to obtain monocyte-derived macrophages, which were further cultured with RANKL for osteoclast differentiation. The RA PBMCs were from RA patients (age ≥ 18 and <70 years) who fulfilled American College of Rheumatology (ACR) 2010 RA classification criteria with disease duration <5 years and were under TNFi therapy for the first time (Enbrel, 25 mg weekly). Experiments with human cells were approved by Nanfang Hospital (China) and the Hospital for Special Surgery (USA) Institutional Review Board. Informed consent (PBMC collection) was obtained from all healthy volunteers and RA patients. All experiments were performed in accordance with relevant guidelines and regulations. TRAP staining was performed with an acid phosphatase leukocyte diagnostic kit (Sigma-Aldrich) in accordance with the manufacturer's instructions.

Actin cytoskeleton reorganization assay. 2×10^4 WT or $G\alpha_{13}^{\Delta M/\Delta M}$ BMMs were cultured on 96 well plates for three days or 6×10^3 WT or $G\alpha_{13}^{\Delta M/\Delta M}$ BMMs on dentin slices (0.4 cm in diameter) for six days with CM (equivalent of 20 ng/ml of rM-CSF) and 40 ng/ml RANKL. The cells were then starved in the culture medium without FBS, M-CSF and RANKL for 5 hours, and were re-stimulated with 20 ng/ml M-CSF and 40 ng/ml RANKL for 0, 5, 15 or 30 minutes as indicated in figure legends. Phalloidin staining was performed in accordance with manufacturer's instructions. Briefly, the cells were fixed with 4% PFA/PBS for 10 min at room temperature (RT) and washed with PBS. Then, the cells were permeabilized in 0.5% Triton X-100/PBS for 5 min followed by blocking with 1% BSA/PBS for 20 min at RT. The cells were then incubated with Alexa Fluor® 488 phalloidin (Invitrogen, 1:500 dilution) for 20 minutes. After washing with PBS, fluorescent signals were detected with a fluorescent microscope. The osteomeasure software (OsteoMetrics, Atlanta, GA, USA) was used for the quantitative analysis of actin ring/podosome belt formation in the cell cultures using standard procedures according to the program's instruction.

***In vitro* adhesion assay.** To prepare fibronectin-coated plates, 6 well plates were incubated with 1 ml of fibronectin (10 μg/ml) per each well for 2 hours at 37 °C. The plates were then washed with PBS for 3 times and were ready for adhesion assay. 8×10^6 WT or $G\alpha13^{\Delta M/\Delta M}$ BMMs were cultured with CM (equivalent of 20 ng/ml of rM-CSF) and 40 ng/ml RANKL on 10 cm culture dishes for 3 days. The cells were then starved in the culture medium without FBS, M-CSF and RANKL for 5 hours, and were lifted by scraper. 2×10^6 cells were then plated on the fibronectin-coated 6 well tissue culture plates (attached cells) or left in αMEM as suspension conditions for 15 min or 30 min, followed by immunoblot analysis or GTP-RhoA pull down assay.

Mineral resorption pit assay. The mineral resorption activity of osteoclasts was examined using 96-well Corning Osteo Assay Surface Plates (Sigma-Aldrich). BMMs were plated at a seeding density of 2×10^4 per well and incubated with CM (equivalent of 20 ng/ml of rM-CSF) and RANKL (40 ng/ml) for 8 days, with medium exchange every day once mature round shaped-osteoclasts were observed. After removing cells with 10% bleach solution, the minerals were stained with von kossa to visualize the formation of resorptive pits. The resorptive area was analyzed using ImageJ (National Institutes of Health, Bethesda, MD, USA).

Reverse transcription and real-time PCR. For quantification of mRNA, reverse transcription and real-time PCR were performed as previously described[40]. Briefly, DNA-free RNA was obtained using the RNeasy

Mini Kit (QIAGEN) with DNase treatment, and total RNA was reverse transcribed using a First Strand cDNA Synthesis Kit (Thermo Fisher Scientific, Waltham, MA, USA). Real-time PCR was performed in triplicate using Fast SYBR® Green Master Mix and the QuantStudio5 Real-Time PCR System (Applied Biosystems, Foster City, CA) following the manufacturer's protocol. Gene expression was normalized relative to the gene expression levels of Glyceraldehyde-3-phosphate dehydrogenease (*Gapdh*). The primer sequences are available upon request.

RNA-seq and Bioinformatics analysis. Total RNA was extracted using RNeasy Mini Kit (QIAGEN) following the manufacturer's instructions. True-seq RNA Library preparation kits (Illumina) were used to purify poly-A+ transcripts and generate libraries with multiplexed barcode adaptors following the manufacturer's instructions. All samples passed quality control analysis using a Bioanalyzer 2100 (Agilent). RNA-seq libraries were constructed per the Illumina TrueSeq RNA sample preparation kit. High-throughput sequencing was performed using the Illumina HiSeq 4000 in the Weill Cornell Medical College Genomics Resources Core Facility. RNA-seq reads were aligned to the mouse genome (mm10) using STAR[41]. HTseq[42]. was subsequently used to count reads in features and then EdgeR[43] was used to estimate the transcript abundances as TPM (transcripts per million) values. Heatmaps were generated by the pheatmap package in R. Gene Ontology (GO) analysis was performed with Panther Classification System[44,45] input with the RANKL-regulated genes that were more highly expressed in $G\alpha13^{\Delta M/\Delta M}$ cells than WT cells ($\geq$1.5 fold). Gα13 regulated pathways by the GO analysis were ranked based on the *p* values. *p* values were calculated following the program's instructions. RNA-seq data (accession #GSE116550) have been deposited in NCBI's Gene Expression Omnibus (http://www.ncbi.nlm.nih.gov/geo/query/acc.cgi?acc=GSE116550).

Immunoblot analysis. Total cell extracts were obtained using lysis buffer containing 150mMTris-HCl (pH 6.8), 6% SDS, 30% glycerol, and 0.03% Bromophenol Blue; 10% 2-ME was added immediately before harvesting cells. Cell lysates were fractionated on 7.5% SDS-PAGE, transferred to Immobilon-P membranes (Millipore), and incubated with specific antibodies. Western Lightning plus-ECL (PerkinElmer) was used for detection. For immunoblotting, anti-NFATc1 (556602, 1:1000 dilution) was from BD Biosciences. Anti-Blimp1 (sc-47732, 1:1000 dilution), anti-Gα13 (sc-410, 1:500 dilution), anti-RhoA (sc-418), and anti-p38α (sc-535, 1:1000 dilution) were purchased from Santa Cruz Biotechnology (Dallas, TX, USA). Anti-pyk2 (06-559, 1:1000 dilution) was from EMD Millipore. Anti-phospho-Pyk2 (Try402) (#3291, 1:1000 dilution), anti-phospho-Akt (Ser473) (#9271, 1:1000 dilution), anti-phospho-Akt (Thr408) (#2965, 1:1000 dilution), anti-Akt (#9272, 1:1000 dilution), anti-phospho-ERK (Ser473) (#9101, 1:1000 dilution), anti-ERK (#9102, 1:1000 dilution), anti-phospho-Src family (Tyr416) (#2101, 1:1000 dilution) were purchased from Cell Signaling Technology Inc. (Danvers, MA, USA). Anti- phospho-Rock2 (Ser1366, 1:500 dilution) is from GeneTex.

Purification of GST-PBD protein. The GST-PBD plasmid[27] was purified as described[46]. Briefly, fusion protein containing RhoA-binding domain Rhotekin (RhBD, amino acids 7–89) fused with GST were produced in *Eschericia coli* BL21 cells. After isopropylthigalactoside (IPTG) induction for 4 hrs at 30 °C, pellets of bacteria were resuspended in Bacterial lysis buffer containing 50 mM Tris–HCl, pH 7.5, 150 mM NaCl, 5 mM MgCl$_2$, 1 mM EDTA, 1 mM dithiothreitol (DTT), 1 mM phenylmethylsulfonyl fluoride (PMSF), and 1 μg/mL aprotinin and then sonicated. Cell lysates were incubated with GST beads (ThermoFisher) for 2 hrs at 4 °C. The beads were wash 5 times with washing buffer containing 50 mM Tris–HCl, pH 7.5, 150 mM NaCl, 5 mM MgCl$_2$, 1 mM EDTA, 1 mM dithiothreitol (DTT), 1 mM PMSF, and 1 μg/mL aprotinin. The beads were aliquoted in wash buffer with 10% v/v glycerol (1:1 slurry) and stored at −80 °C.

Affinity- precipitation of cellular GTP-RhoA (pulldown assay). The suspension and attached osteoclasts from adhesion assay were lysed in a buffer containing 50 mM Tris/HCl, pH 7.5, 1 mM EDTA, 500 mM NaCl, 10 mM MgCl$_2$, 1% Triton X-100, and protease inhibitors (4 μg/ml leupeptin, 5 μg/ml apropeptin, 1 mM PMSF, 5 mM NaF, 5 mM sodium orthovanadate and protease inhibitor cocktail). Cell lysates were clarified by centrifugation at 15 000 g at 4 °C for 10 min. Equal volumes of lysates were incubated with 50 μg GST–RBD fusion protein at 4 °C for 1 hr while rotating. After pulldown, the beads were centrifuged at 250 g for 2 min and 4 °C and then washed five times with a buffer containing 50 mM Tris/HCl, pH 7.5, 150 mM NaCl, 10 mM MgCl$_2$, 1% Triton X-100, 10 μg/ml leupeptin, 10 μg/ml apropeptin and 1 mM PMSF. The pulled down active RhoA proteins were analyzed by SDS-PAGE followed by immunoblotting against RhoA (Santa Cruz Biotechnology, sc-418). ImageJ was used to quantify the immunoblot band density that reflects the amount of proteins, and the relative amount of GTP-bound RhoA was normalized to the total amount of RhoA in cell lysates for the comparison of RhoA activity in different samples.

Statistical analysis. Statistical analysis was performed using Graphpad Prism® software. The two-tailed Student's *t* test was applied when there were only two groups of samples. In the case of more than two groups of samples, one-way ANOVA was used with one condition, and two-way ANOVA was used with more than two conditions. ANOVA analysis was followed by Post hoc Bonferroni's correction for multiple comparisons. $p < 0.05$ was taken as statistically significant; *p value < 0.05, **p value < 0.01 and ***p value < 0.001. Data are presented as the mean $\pm$ SD as indicated in the figure legends.

References

1. Goldring, S. R. *et al.* Bone remodelling in inflammatory arthritis. *Annals of the rheumatic diseases* **72**(Suppl 2), ii52–55, https://doi.org/10.1136/annrheumdis-2012-202199 (2013).
2. Novack, D. V. & Teitelbaum, S. L. The osteoclast: friend or foe? *Annual review of pathology* **3**, 457–484, https://doi.org/10.1146/annurev.pathmechdis.3.121806.151431 (2008).

3. Schett, G. & Gravallese, E. Bone erosion in rheumatoid arthritis: mechanisms, diagnosis and treatment. *Nature reviews. Rheumatology* **8**, 656–664, https://doi.org/10.1038/nrrheum.2012.153 (2012).
4. Teitelbaum, S. L. Osteoclasts; culprits in inflammatory osteolysis. *Arthritis research & therapy* **8**, 201, https://doi.org/10.1186/ar1857 (2006).
5. Mbalaviele, G., Novack, D. V., Schett, G. & Teitelbaum, S. L. Inflammatory osteolysis: a conspiracy against bone. *The Journal of clinical investigation* **127**, 2030–2039, https://doi.org/10.1172/JCI93356 (2017).
6. Asagiri, M. & Takayanagi, H. The molecular understanding of osteoclast differentiation. *Bone* **40**, 251–264, https://doi.org/10.1016/j.bone.2006.09.023 (2007).
7. Zhao, B. & Ivashkiv, L. B. Negative regulation of osteoclastogenesis and bone resorption by cytokines and transcriptional repressors. *Arthritis research & therapy* **13**, 234, https://doi.org/10.1186/ar3379 (2011).
8. Humphrey, M. B., Lanier, L. L. & Nakamura, M. C. Role of ITAM-containing adapter proteins and their receptors in the immune system and bone. *Immunological reviews* **208**, 50–65, https://doi.org/10.1111/j.0105-2896.2005.00325.x (2005).
9. Boyce, B. F. Advances in the regulation of osteoclasts and osteoclast functions. *Journal of dental research* **92**, 860–867, https://doi.org/10.1177/0022034513500306 (2013).
10. Yagi, M. *et al.* DC-STAMP is essential for cell-cell fusion in osteoclasts and foreign body giant cells. *The Journal of experimental medicine* **202**, 345–351, https://doi.org/10.1084/jem.20050645 (2005).
11. Lee, S. H. *et al.* V-ATPase V0 subunit d2-deficient mice exhibit impaired osteoclast fusion and increased bone formation. *Nature medicine* **12**, 1403–1409, https://doi.org/10.1038/nm1514 (2006).
12. Vaananen, H. K., Zhao, H., Mulari, M. & Halleen, J. M. The cell biology of osteoclast function. *Journal of cell science* **113**(Pt 3), 377–381 (2000).
13. Teitelbaum, S. L. The osteoclast and its unique cytoskeleton. *Annals of the New York Academy of Sciences* **1240**, 14–17, https://doi.org/10.1111/j.1749-6632.2011.06283.x (2011).
14. Zou, W. & Teitelbaum, S. L. Integrins, growth factors, and the osteoclast cytoskeleton. *Annals of the New York Academy of Sciences* **1192**, 27–31, https://doi.org/10.1111/j.1749-6632.2009.05245.x (2010).
15. Novack, D. V. & Faccio, R. Osteoclast motility: putting the brakes on bone resorption. *Ageing research reviews* **10**, 54–61, https://doi.org/10.1016/j.arr.2009.09.005 (2011).
16. Martin, T., Gooi, J. H. & Sims, N. A. Molecular mechanisms in coupling of bone formation to resorption. *Critical reviews in eukaryotic gene expression* **19**, 73–88 (2009).
17. Sims, N. A. & Martin, T. J. Coupling the activities of bone formation and resorption: a multitude of signals within the basic multicellular unit. *BoneKEy reports* **3**, 481, https://doi.org/10.1038/bonekey.2013.215 (2014).
18. Takeshita, S. *et al.* Osteoclast-secreted CTHRC1 in the coupling of bone resorption to formation. *The Journal of clinical investigation* **123**, 3914–3924, https://doi.org/10.1172/JCI69493 (2013).
19. Cusick, T. *et al.* Odanacatib treatment increases hip bone mass and cortical thickness by preserving endocortical bone formation and stimulating periosteal bone formation in the ovariectomized adult rhesus monkey. *Journal of bone and mineral research: the official journal of the American Society for Bone and Mineral Research* **27**, 524–537, https://doi.org/10.1002/jbmr.1477 (2012).
20. Kurose, H. Galpha12 and Galpha13 as key regulatory mediator in signal transduction. *Life sciences* **74**, 155–161 (2003).
21. Syrovatkina, V., Alegre, K. O., Dey, R. & Huang, X. Y. Regulation, Signaling, and Physiological Functions of G-Proteins. *Journal of molecular biology* **428**, 3850–3868, https://doi.org/10.1016/j.jmb.2016.08.002 (2016).
22. Offermanns, S., Mancino, V., Revel, J. P. & Simon, M. I. Vascular system defects and impaired cell chemokinesis as a result of Galpha13 deficiency. *Science* **275**, 533–536 (1997).
23. Ruppel, K. M. *et al.* Essential role for Galpha13 in endothelial cells during embryonic development. *Proceedings of the National Academy of Sciences of the United States of America* **102**, 8281–8286, https://doi.org/10.1073/pnas.0503326102 (2005).
24. Wu, M. *et al.* Galpha13 negatively controls osteoclastogenesis through inhibition of the Akt-GSK3beta-NFATc1 signalling pathway. *Nature communications* **8**, 13700, https://doi.org/10.1038/ncomms13700 (2017).
25. Wang, L. *et al.* G-Protein Galpha13 Functions with Abl Kinase to Regulate Actin Cytoskeletal Reorganization. *Journal of molecular biology* **429**, 3836–3849, https://doi.org/10.1016/j.jmb.2017.10.020 (2017).
26. Wang, D. *et al.* G proteins G12 and G13 control the dynamic turnover of growth factor-induced dorsal ruffles. *The Journal of biological chemistry* **281**, 32660–32667, https://doi.org/10.1074/jbc.M604588200 (2006).
27. Shan, D. *et al.* The G protein G alpha(13) is required for growth factor-induced cell migration. *Developmental cell* **10**, 707–718, https://doi.org/10.1016/j.devcel.2006.03.014 (2006).
28. Chen, L., Zhang, J. J., Rafii, S. & Huang, X. Y. Suppression of tumor angiogenesis by Galpha(13) haploinsufficiency. *The Journal of biological chemistry* **284**, 27409–27415, https://doi.org/10.1074/jbc.M109.025460 (2009).
29. Rustad, K. C., Wong, V. W. & Gurtner, G. C. The role of focal adhesion complexes in fibroblast mechanotransduction during scar formation. *Differentiation; research in biological diversity* **86**, 87–91, https://doi.org/10.1016/j.diff.2013.02.003 (2013).
30. Zhang, Y. *et al.* PGC1beta Organizes the Osteoclast Cytoskeleton by Mitochondrial Biogenesis and Activation. *Journal of bone and mineral research: the official journal of the American Society for Bone and Mineral Research* **33**, 1114–1125, https://doi.org/10.1002/jbmr.3398 (2018).
31. Koo, J. H. *et al.* Galpha13 ablation reprograms myofibers to oxidative phenotype and enhances whole-body metabolism. *The Journal of clinical investigation* **127**, 3845–3860, https://doi.org/10.1172/JCI92067 (2017).
32. Matsuo, K. & Irie, N. Osteoclast-osteoblast communication. *Archives of biochemistry and biophysics* **473**, 201–209, https://doi.org/10.1016/j.abb.2008.03.027 (2008).
33. Raggatt, L. J. & Partridge, N. C. Cellular and molecular mechanisms of bone remodeling. *The Journal of biological chemistry* **285**, 25103–25108, https://doi.org/10.1074/jbc.R109.041087 (2010).
34. Bartolak-Suki, E., Imsirovic, J., Nishibori, Y., Krishnan, R. & Suki, B. Regulation of Mitochondrial Structure and Dynamics by the Cytoskeleton and Mechanical Factors. *International journal of molecular sciences* **18**, https://doi.org/10.3390/ijms18081812 (2017).
35. Kozasa, T. *et al.* p115 RhoGEF, a GTPase activating protein for Galpha12 and Galpha13. *Science* **280**, 2109–2111 (1998).
36. Whyte, L. S. *et al.* The putative cannabinoid receptor GPR55 affects osteoclast function *in vitro* and bone mass *in vivo. Proceedings of the National Academy of Sciences of the United States of America* **106**, 16511–16516, https://doi.org/10.1073/pnas.0902743106 (2009).
37. Ryberg, E. *et al.* The orphan receptor GPR55 is a novel cannabinoid receptor. *British journal of pharmacology* **152**, 1092–1101, https://doi.org/10.1038/sj.bjp.0707460 (2007).
38. Li, S. *et al.* RBP-J imposes a requirement for ITAM-mediated costimulation of osteoclastogenesis. *The Journal of clinical investigation* **124**, 5057–5073, https://doi.org/10.1172/JCI71882 (2014).
39. Bouxsein, M. L. *et al.* Guidelines for assessment of bone microstructure in rodents using micro-computed tomography. *Journal of bone and mineral research: the official journal of the American Society for Bone and Mineral Research* **25**, 1468–1486, https://doi.org/10.1002/jbmr.141 (2010).
40. Zhao, B. *et al.* Interferon regulatory factor-8 regulates bone metabolism by suppressing osteoclastogenesis. *Nature medicine* **15**, 1066–1071, https://doi.org/10.1038/nm.2007 (2009).
41. Dobin, A. *et al.* STAR: ultrafast universal RNA-seq aligner. *Bioinformatics* **29**, 15–21, https://doi.org/10.1093/bioinformatics/bts635 (2013).
42. Anders, S., Pyl, P. T. & Huber, W. HTSeq–a Python framework to work with high-throughput sequencing data. *Bioinformatics* **31**, 166–169, https://doi.org/10.1093/bioinformatics/btu638 (2015).

43. Robinson, M. D., McCarthy, D. J. & Smyth, G. K. EdgeR: a Bioconductor package for differential expression analysis of digital gene expression data. *Bioinformatics* **26**, 139–140, https://doi.org/10.1093/bioinformatics/btp616 (2010).
44. Thomas, P. D. *et al.* PANTHER: a library of protein families and subfamilies indexed by function. *Genome research* **13**, 2129–2141, https://doi.org/10.1101/gr.772403 (2003).
45. Thomas, P. D. *et al.* PANTHER: a browsable database of gene products organized by biological function, using curated protein family and subfamily classification. *Nucleic acids research* **31**, 334–341 (2003).
46. Jennings, R. T. & Knaus, U. G. Rho family and Rap GTPase activation assays. *Methods in molecular biology* **1124**, 79–88, 10.1007/978-1-62703-845-4_6 (2014).

Acknowledgements

Author Contributions

S.N., K.I. C.X. and Z.D. performed most of the experiments. K.I. analyzed RNAseq data, designed experiments and analyzed data. V.S. performed RhoA pull down experiments. G.V. assisted cell culture experiments. L.Z. performed the human R.A. cell experiments. X.-Y.H. contributed to data interpretation and discussion. S.N. and K.I. contributed to manuscript preparation. B.Z. conceived, designed, supervised the project and wrote the manuscript.

Additional Information

Supplementary information accompanies this paper at https://doi.org/10.1038/s41598-019-40974-z.

Competing Interests: The authors declare no competing interests.

Publisher's note: Springer Nature remains neutral with regard to jurisdictional claims in published maps and institutional affiliations.